

Interferometric signatures of the temperature dependence of the specific shear viscosity in heavy-ion collisions

Christopher Plumberg¹ and Ulrich Heinz¹

¹*Department of Physics, The Ohio State University, Columbus, OH 43210-1117, USA*

(Dated: April 9, 2015)

Recent work has shown that a temperature dependence of the shear viscosity to entropy ratio, η/s , influences the collective flow pattern in heavy-ion collisions in characteristic ways that can be measured by studying hadron transverse momentum spectra and their anisotropies. Here we point out that it also affects the pair momentum dependence of the Hanbury-Brown-Twiss (HBT) radii (the source size parameters extracted from two-particle intensity interferometry) and the variance of their event-by-event fluctuations. This observation establishes interferometric signatures as useful observables to complement the constraining power of single-particle spectra on the temperature dependence of η/s .

PACS numbers: 25.75.-q, 12.38.Mh, 25.75.Ld, 24.10.Nz

I. INTRODUCTION

Recently, a great deal of theoretical attention has been devoted to the accurate determination of the shear-viscosity-to-entropy-density ratio (η/s) of the quark-gluon plasma (QGP) and the hadron resonance gas (HRG), and how its temperature dependence around the transition point between these two phases might be probed in heavy-ion collisions. In particular, a recent study [1] suggested the possibility of discriminating experimentally between different parametrizations of the temperature dependence of η/s using systematic analyses of the anisotropic flows v_2 and v_4 as functions of transverse momentum p_T and pseudorapidity η . In this paper, we present a complementary analysis of the HBT radii for Au+Au collisions at RHIC energies, to argue that the HBT radii can be used profitably to help constrain viable parametrizations of $(\eta/s)(T)$.

The HBT radii are physical observables which are well defined on an event-by-event basis. As parameters that describe the size and shape of the particle emitting source, they fluctuate from event to event. Experimental data so far [2–7] determine only the average source radii characterizing a large ensemble of events [8]. Elsewhere [9] we discuss new ideas of how to complement such measurements of the ensemble-averaged HBT radii by a determination of their variances, i.e., the width parameters characterizing their event-by-event fluctuations. In that work [9] it is also shown that the experimentally accessible observables characterizing the mean source radii and their variances clearly track the algebraic mean and variance of the source radii that are calculated theoretically from the individual emission functions of a large set of dynamically simulated heavy-ion collisions with fluctuating initial conditions. We here show the transverse pair momentum (\vec{K}_T) dependencies of these mean radii and their variances for the same four parametrizations of the specific shear viscosity η/s studied in [1]. We also compare the mean radii to those one would obtain from a single average source by dynamically evolving a single initial profile, constructed as the ensemble average of the

fluctuating initial conditions of the full ensemble.

To save time and effort, we employ for this pioneering study the shortcut of calculating the HBT radii from the source variances of the emission function [10–13] for directly emitted pions only, instead of performing a 3-D Gaussian fit to the correlation function including all resonance decays [13–16]. This approximation, which holds exactly only for Gaussian sources [12], is known to be sufficient to discern qualitative features of the HBT radii and their K_T dependences, although it is not accurate enough for quantitative comparisons with experimental data [17].

II. ANALYSIS

A. Initial conditions

In this paper, we compute the HBT radii, as outlined in the previous section, for central (0-10%) Au+Au collisions at 200 A GeV, based on charged pion correlations. We use the iEBE-VISHNU package [18] in modeling the evolution of heavy-ion collisions. For the (hydrodynamical) initial conditions of the fireball, we employ the MC-Glauber model [19] with p+p multiplicity fluctuations [18] to generate the initial entropy density distribution in the transverse plane. The subsequent dynamical evolution is performed on an event-by-event basis, meaning that each set of initial conditions that we generate initializes one of the N_{ev} hydrodynamically evolved events in our ensemble. In this paper, we take $N_{\text{ev}} = 1000$.

B. Hydrodynamic evolution and $(\eta/s)(T)$

We perform the hydrodynamical evolution of the initial conditions with the VISH2+1 code [20], using the s95p-PCE165-v0 equation of state [21]. We choose this evolution to begin at an initial proper time $\tau_0 = 0.6 \text{ fm}/c$, where $\tau = 0$ corresponds to the instant at which the two

nuclei collide. Also, although necessary for quantitatively precise comparisons with experimental data [22], we do not incorporate here any initial transverse flow into the hydrodynamical evolution.

For our study, we use for $(\eta/s)(T)$ one of the four parametrizations given in [1]:

- LH-LQ, in which $(\eta/s)(T) = 0.08$ for all T ;
- LH-HQ, in which $(\eta/s)(T) = 0.08$ for $T \leq T_{\text{tr}}$ and

$$(\eta/s)(T)_{\text{QGP}} = -0.289 + 0.288 \frac{T}{T_{\text{tr}}} + 0.0818 \left(\frac{T}{T_{\text{tr}}} \right)^2, \quad \text{for } T > T_{\text{tr}}; \quad (1)$$

- HH-LQ, in which $(\eta/s)(T) = 0.08$ for $T > T_{\text{tr}}$ and

$$(\eta/s)(T)_{\text{HRG}} = 0.681 - 0.0594 \frac{T}{T_{\text{tr}}} - 0.544 \left(\frac{T}{T_{\text{tr}}} \right)^2 \quad \text{for } T \leq T_{\text{tr}}; \quad (2)$$

- HH-HQ, for which we use $(\eta/s)(T)_{\text{HRG}}$ for $T \leq T_{\text{tr}}$ and $(\eta/s)(T)_{\text{QGP}}$ for $T > T_{\text{tr}}$.

Here, $T_{\text{tr}} = 180$ MeV [1] represents the transition temperature between the QGP and HRG phases. The four parametrizations are shown in Fig. 1.

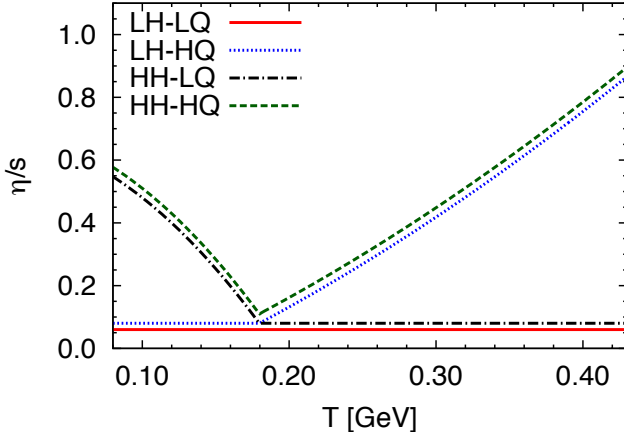


FIG. 1: The different parametrizations of $(\eta/s)(T)$ used in this work, taken from [1].

As also pointed out in [1], for identical initial conditions viscous entropy production generates different final multiplicities for different choices of $(\eta/s)(T)$. This effect is especially severe for the parametrizations LH-HQ and HH-HQ where at early times, when the longitudinal-transverse velocity shear is biggest, $(\eta/s)(T)$ is very large. To compensate for this effect, we rescale our initial entropy profiles by a constant factor κ_{fit} , which depends on the chosen parametrization of $(\eta/s)(T)$. For a given choice of $(\eta/s)(T)$, κ_{fit} is chosen so that an ensemble-averaged initial entropy profile always reproduces the

same final thermal π^+ multiplicity.¹ Normalizing all of the averaged profiles to the ideal fluid case (which thus corresponds to $\kappa_{\text{fit}} = 1$) we find

- LH-LQ: $\kappa_{\text{fit}} = 0.889$
- LH-HQ: $\kappa_{\text{fit}} = 0.596$
- HH-LQ: $\kappa_{\text{fit}} = 0.878$
- HH-HQ: $\kappa_{\text{fit}} = 0.589$

As expected, parametrizations with a large plasma viscosity require a significant suppression of the initial entropy density profile in order to compensate for viscous heating and to reproduce the measured final multiplicities in Au+Au collisions at RHIC energies. Finally, we terminate the hydrodynamical evolution on a decoupling surface (the "freeze-out surface") of constant temperature $T_{\text{dec}} = 120$ MeV.

C. Pion emission function at freeze-out

On the freeze-out surface for each event, the pion emission function is defined by the Cooper-Frye integral [23–25]

$$S(x, p) = \frac{1}{(2\pi)^3} \int_{\Sigma} p \cdot d^3\sigma(y) \delta^4(x-y) f(y, p), \quad (3)$$

$$f(x, p) = f_0(x, p) + \delta f(x, p)$$

$$= \frac{1}{e^{(p \cdot u - \mu)/T} - 1} + \frac{p^\mu p^\nu \pi_{\mu\nu}}{2T^2(e + \mathcal{P})} f_0(1 + f_0). \quad (4)$$

Here, δf is the first-order viscous corrections to the ideal distribution function f_0 [26, 27] for which we assume a quadratic dependence on p . $\pi_{\mu\nu}(x)$ and $u^\mu(x)$ are the shear stress and flow velocity profiles along the freeze-out surface Σ , respectively. μ , T , e , and \mathcal{P} are the chemical potential, decoupling temperature, energy density, and pressure, respectively, which are all constant on Σ by construction. $d^3\sigma_\mu(x)$ is the outward pointing normal vector on Σ at point x .

D. Ensemble averaging

Theoretically, the HBT radii may be defined for either a single event or an ensemble containing many events. Due to statistical limitations arising from the finite number of particles emitted in a single event, precise measurements of the full set of HBT radii and their K_T de-

¹ Since we always decouple at the same constant freeze-out temperature, $\frac{dN_{\pi^+}}{d\eta}$ is a fixed fraction of the total multiplicity $\frac{dN_{\text{ch}}}{d\eta}$. Therefore, this normalization ensures that, on average, all events have the same final charged multiplicity.

pendences for a single event are not possible [8]. Three-dimensional experimental HBT analyses, therefore, exclusively report measurements based on large collections of events, rather than measurements of event-by-event HBT radii. In order to obtain an apples-to-apples comparison with experimental data, theoretical HBT calculations must therefore, at some level, average over all events in the ensemble.

This procedure, known as *ensemble averaging*, can be performed in several ways, two of which we consider here. According to one prescription, the initial conditions for all events in the ensemble are averaged *before* their hydrodynamical evolution. We refer to this method of ensemble averaging as "single-shot hydrodynamics" (SSH) [30]. For a sufficiently large ensemble, averaging over many, individually fluctuating and bumpy initial conditions results in a *smooth* initial transverse entropy density profile, which in turn may be evolved hydrodynamically as a single, averaged event. This prescription eliminates any sensitivity to event-by-event fluctuations in the initial state. We will here denote the HBT radii derived from single-shot hydrodynamics by \bar{R}_{ij}^2 ($i, j = o, s, l$).

An alternative prescription for computing the ensemble-averaged HBT radii evolves each fluctuating event *independently* and averages over the entire ensemble only *after* the HBT radii have been computed for each event from its individual hydrodynamic emission function $S(x, K)$. This leads to the following definition of ensemble-averaged HBT radii:

$$\langle R_{ij}^2 \rangle \equiv \frac{1}{N_{\text{ev}}} \sum_{k=1}^{N_{\text{ev}}} (R_{ij}^2)_k. \quad (5)$$

We denote by $(R_{ij}^2)_k$ the HBT radii of the k th event, and we label the mean HBT radii computed according to this "direct ensemble average" (DEA) by $\langle R_{ij}^2 \rangle$.

E. HBT calculations

The basic formalism describing our calculation of the HBT radii was presented in [8]. Once the emission function (3) for a particular event has been obtained from the hydrodynamic output using Eq. (4), the HBT radii corresponding to that emission function may be defined by [10, 12]

$$R_{ij}^2(\vec{K}) = \langle (\tilde{x}_i - \beta_i \tilde{t})(\tilde{x}_j - \beta_j \tilde{t}) \rangle_S, \quad (6)$$

where $\tilde{x}_\mu = x_\mu - \langle x_\mu \rangle_S$, $\vec{\beta} = \vec{K}/E_K$, $E_K = \sqrt{m_\pi^2 + \vec{K}^2}$, and the \vec{K} dependence of R_{ij}^2 arises from the \vec{K} dependence of the emission function in the definition of the source average:

$$\langle f(x) \rangle_S \equiv \frac{\int d^4x f(x) S(x, K)}{\int d^4x S(x, K)}. \quad (7)$$

$\vec{K} = (K_T, \Phi_K, Y)$ is the average pair momentum in the lab frame, $\vec{K} = \frac{1}{2}(\vec{p}_1 + \vec{p}_2)$. In this paper, we consider only pairs of identical particles at mid-rapidity ($Y = 0$).

The dependence of the HBT radii on the pair emission angle Φ_K also allows them to be expanded in a Fourier series (we suppress the additional dependence of all HBT parameters on K_T and Y),

$$R_{ij}^2(\Phi_K) = R_{ij,0}^2 + 2 \sum_{n=1}^{\infty} \left[R_{ij,n}^{2(c)} \cos(n(\Phi_K - \Psi_n)) + R_{ij,n}^{2(s)} \sin(n(\Phi_K - \Psi_n)) \right], \quad (8)$$

where the flow-plane angle Ψ_n is defined by the complex phase of the n th-order anisotropic flow coefficient v_n [31]:

$$v_n e^{in\Psi_n} \equiv \langle e^{in\Phi} \rangle = \frac{\int_0^\infty dK_T K_T \int_{-\pi}^\pi d\Phi_K e^{in\Phi_K} \int d^4x S(x, K)}{\int_0^\infty dK_T K_T \int_{-\pi}^\pi d\Phi_K \int d^4x S(x, K)}. \quad (9)$$

In this work, we average R_s^2 , R_o^2 , and R_l^2 over Φ_K , but we report the 2nd Φ_K -harmonic $R_{os,2}^2$ of the out-side cross-term $R_{os}^2(\Phi_K)$, since the mean value of its Φ_K -average $\langle R_{os,0}^2 \rangle$ vanishes for symmetric nucleus-nucleus collisions at midrapidity [32]. For single events with fluctuating initial conditions, $R_{os,2}^2$ receives non-zero contributions from both $R_{os,2}^{2(c)}$ and $R_{os,2}^{2(s)}$ on an event-by-event basis, but the former contribution averages to zero for a sufficiently large ensemble. We therefore consider only the mean and variance of the event-wise fluctuations of $R_{os,2}^{2(s)} \equiv R_{os,2}^2$ for the remainder of this paper. For notational simplicity, we will drop the '0' subscript from the azimuthally averaged radii, and write simply R_{ij}^2 ($i, j = o, s, l$).

At $Y = 0$, Eq. (6) gives

$$R_s^2 = \langle \tilde{x}_s^2 \rangle_S, \quad R_l^2 = \langle \tilde{x}_l^2 \rangle_S. \quad (10)$$

R_s^2 and R_l^2 thus depend only on the geometric aspects of the emission function. By contrast, both R_o^2 and R_{ol}^2 involve a combination of spatial and temporal source variances:

$$R_o^2 = \langle \tilde{x}_o^2 \rangle_S - 2\beta_T \langle \tilde{x}_o \tilde{t} \rangle_S + \beta_T^2 \langle \tilde{t}^2 \rangle_S, \quad (11)$$

$$R_{os}^2 = \langle \tilde{x}_o \tilde{x}_s \rangle_S - \beta_T \langle \tilde{x}_s \tilde{t} \rangle_S \quad (12)$$

In [9] we describe a method for experimentally measuring, in addition to the mean, also the variance of an event-by-event distribution of the HBT radii. As a prediction for such measurements, we here also compute the variances of the HBT radii for our ensemble of $N_{\text{ev}} = 1000$ events, defined by²

$$\sigma_{ij}^2 = \frac{1}{N_{\text{ev}} - 1} \sum_{k=1}^{N_{\text{ev}}} \left((R_{ij}^2)_k - \langle R_{ij}^2 \rangle \right)^2. \quad (13)$$

² The factor $\frac{1}{N_{\text{ev}} - 1}$ makes σ_{ij}^2 an unbiased estimator of the true variance of the event-by-event distribution of HBT radii [33].

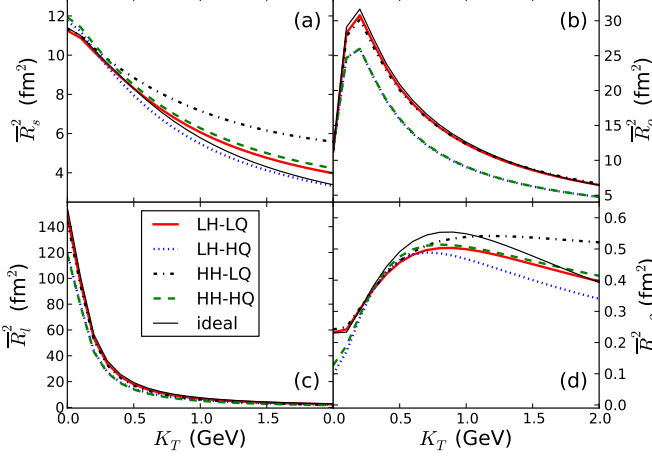


FIG. 2: \bar{R}_{ij}^2 vs. K_T from single-shot hydrodynamics, for ideal and viscous fluids with the temperature dependent shear viscosities $(\eta/s)(T)$ shown in Fig. 1. Note the almost perfect overlap of the green (dashed) and blue (dotted) curves in panels (b,c).

In this paper, we will use and plot $\sigma_{ij}/\langle R_{ij}^2 \rangle$ as a measure for the widths of the HBT radii distributions. For the quantity $R_{os,2}^2$, we define the corresponding variance to be

$$\sigma_{os,2}^2 = \frac{1}{N_{ev}-1} \sum_{k=1}^{N_{ev}} \left((R_{os,2}^2)_k - \langle R_{os,2}^2 \rangle \right)^2. \quad (14)$$

III. RESULTS

A. Mean HBT radii and their K_T dependence

In this subsection, we present the mean HBT radii computed according to the two averaging prescriptions described above (single-shot hydrodynamics (SSH) and the direct ensemble average (DEA)), and study their sensitivity to the temperature dependence of the specific shear viscosity $(\eta/s)(T)$.

First we consider in Fig. 2 the radii \bar{R}_{ij}^2 extracted from single-shot hydrodynamics which averages over event-by-event fluctuations in the initial state. Panels (a) and (d) show that the sideward radius \bar{R}_s^2 and the out-side cross term $\bar{R}_{os,2}^2$ exhibit sensitivity to the temperature dependence of $(\eta/s)(T)$ both below and above T_{tr} . However, $(\eta/s)(T)$ affects hadronic observables in two distinct ways. First, there is the cumulative dynamical effect of shear viscosity on the development of flow in the fireball; flow probes the entire temperature history of $(\eta/s)(T)$ between the initial and decoupling temperatures. Second, the emission function is affected by the viscous correction δf to the distribution function at freeze-out, Eq. (4), which is controlled by the value of

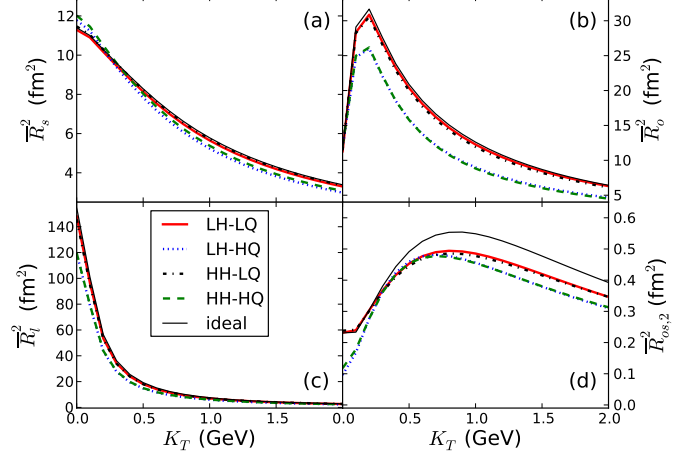


FIG. 3: Same as Fig. 2, but leaving out in Eq. (4) the viscous correction δf at freeze-out. Comparison of Figs. 2a,d and 3a,d shows that the sensitivity of $\bar{R}_s^2(K_T)$ and $\bar{R}_{os,2}^2(K_T)$ to the temperature dependence of $(\eta/s)(T)$ below T_{tr} is almost entirely due to the theoretically poorly controlled viscous correction δf at freeze-out, and that any sensitivity to the temperature dependence of $(\eta/s)(T)$ during the dynamical evolution, i.e. *before freeze-out*, is strongly weighted at high temperatures, i.e. early times. The sensitivity to δf at freeze-out of the HBT radii probing the outward and longitudinal dimensions of the emission function (panels (b,c)) is negligible.

$(\eta/s)(T)$ on the freeze-out surface. This gives a contribution to observables such as the HBT radii that depends exclusively on the behavior of $(\eta/s)(T)$ at T_{dec} and is basically independent of its prior history (except for the accumulated effect of $(\eta/s)(T)$ on the flow pattern whose associated shear tensor also affects the shear stress at freeze-out). To separate the two effects, we plot in Fig. 3 the HBT radii computed without the δf correction, so that only the cumulative dynamical effects of $(\eta/s)(T)$ remain. Figures 3a,d show that deleting δf removes all sensitivity of the sideward and out-side HBT radii on the shear viscosity in the hadronic phase, leaving only a weak sensitivity on the behavior of $(\eta/s)(T)$ in the high-temperature QGP phase.

On the other hand, comparison of panels (b,c) in Figs. 2 and 3 reveals that the outward and longitudinal HBT radii are almost completely unaffected by the behavior of $(\eta/s)(T)$ below T_{tr} and, in particular, receive no significant contribution from the viscous correction δf at freeze-out. This finding is at variance with the results reported in Teaney's pioneering analysis [26] of δf -effects on the HBT radii. We note, however, that Teaney's analysis was based on a blast-wave parametrization of the hydrodynamic flow profile at freeze-out, rather than the profile from a genuine hydrodynamic simulation of the flow. It was noted before in Appendix E of Ref. [20] that δf is very sensitive to the details of the velocity

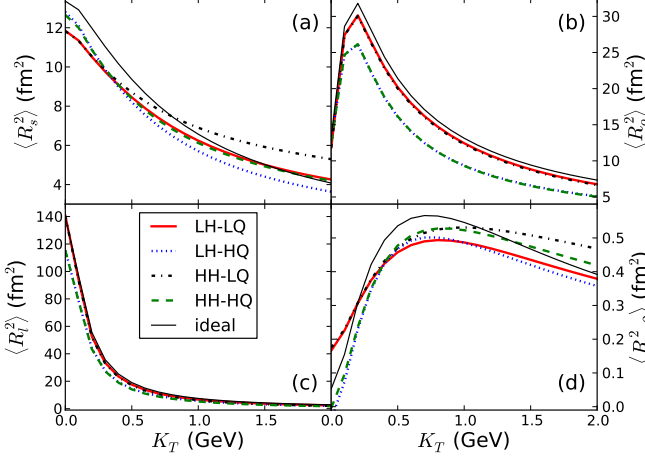


FIG. 4: The ensemble averaged $\langle R_{ij}^2 \rangle$ as a function of pair momentum K_T , for the same choices of $(\eta/s)(T)$ as in Figs. 2 and 3. This figure should be compared with Fig. 2.

shear tensor at freeze-out, and even its sign is fragile. Furthermore, there are well-known conceptual uncertainties about the correct form of δf , especially its p_T dependence [27]. These uncertainties render suspect any observable that strongly depends on δf at freeze-out.³ Therefore, we caution the reader not to trust the apparent sensitivity in Fig. 2a,d of $\bar{R}_s^2(K_T)$ and $\bar{R}_{os,2}^2(K_T)$ to the behavior of $(\eta/s)(T)$ in the hadronic phase. On the other hand, the sensitivity of $\bar{R}_o^2(K_T)$ and $\bar{R}_l^2(K_T)$ exclusively to the temperature dependence of $(\eta/s)(T)$ in the QGP phase *above* T_{tr} appears to be robust and unaffected by freeze-out uncertainties related to δf . These high-temperature effects of $(\eta/s)(T)$ on \bar{R}_o^2 and \bar{R}_l^2 are not huge, but they can reach 20% (for the squared HBT radii) for a range of K_T values below 1.5 GeV.

Studies such as [15, 16] have explored the sensitivity of the HBT radii to shear viscosity using constant (T -independent) η/s and varying that constant. Different from our approach here, when changing η/s they also changed other hydrodynamic parameters to ensure that not only the normalization but also the slope of the p_T -spectra was held fixed. Additionally, both of these studies extract the HBT radii from a Gaussian fit to the full three-dimensional correlation function instead of using

³ We comment that δf -related uncertainties may also affect some of the conclusions in Ref. [1] about the dependence of charged hadron elliptic and quadrangular flow, $v_2^{\text{ch}}(p_T)$ and $v_4^{\text{ch}}(p_T)$, on the behavior of $(\eta/s)(T)$ in the hadronic phase. For example, we found that, when calculated without the δf correction, almost all sensitivity of $v_2(p_T)$ of directly emitted (“thermal”) pions to the temperature dependence of $(\eta/s)(T)$ in the hadronic phase disappears, leaving only a (significantly weaker, but robust) dependence of this observable to the temperature dependence of $(\eta/s)(T)$ in the QGP phase above T_{tr} .

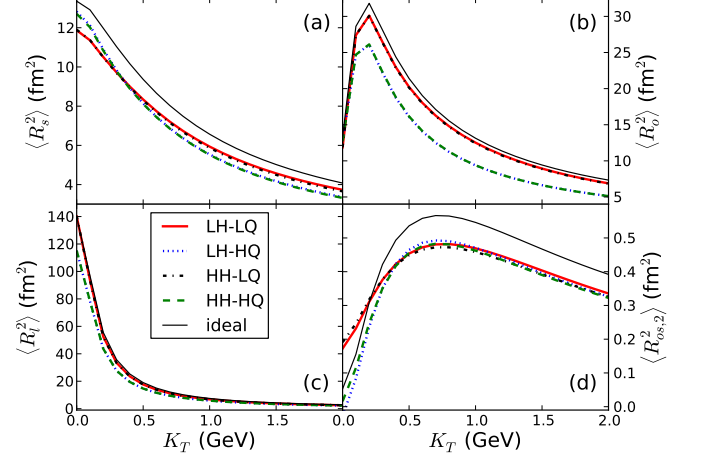


FIG. 5: Same as Fig. 4, but without the δf correction. This figure should be compared with Fig. 3.

the short-cut through the source variances. These differences make a direct comparison of our work with their results difficult. Our findings are qualitatively supported by the work [28] (whose authors, like us, used the source variances method) where it was found that an increase in the Knudsen number (or, equivalently, η/s) resulted in a decrease in R_o^2 . The purpose of the present work is not a realistic comparison with experimental data which, as done in [15, 16], would require a simultaneous tuning of several additional parameters (see also Ref. [29]). Our goal is to check systematically the sensitivity of the HBT radii to a possible T -dependence of η/s , in particular in the context of event-by-event source fluctuations. It is to these fluctuations that we turn our attention next.

We now investigate how the mean HBT radii are affected by event-by-event fluctuations in the initial conditions. To do so we evolve 1000 central (0-10% centrality) Au+Au events at $\sqrt{s} = 200$ A GeV with fluctuating initial conditions and average their correspondingly fluctuating HBT radii after freeze-out, as described in Sec. IID. The results are presented in Fig. 4 (including the full distribution function (4) at freeze-out) and Fig. 5 (without the viscous δf correction in (4) at freeze-out). Compared to Figs. 2 and 3, we see no qualitative differences. Again, robust (although not very strong) sensitivities to the temperature dependence of $(\eta/s)(T)$ *above* T_{tr} are seen in all radii, but for R_s^2 these are buried by a stronger sensitivity to the viscous δf correction at freeze-out (which, we reiterate, is theoretically not well controlled). As was the case for the \bar{R}_{ij}^2 from single-shot hydrodynamics, the δf corrections to the $\langle R_{ij}^2 \rangle$ are negligible when $i, j = o, l$.

In Fig. 6 we plot the fractional change $(\langle R_{ij}^2 \rangle - \bar{R}_{ij}^2) / \bar{R}_{ij}^2$ of the mean squared HBT radii arising from event-by-event fluctuations, as a function of pair momentum. Generically, event-by-event fluctuations are seen to boost the Φ_K -averaged means of the fluctuating

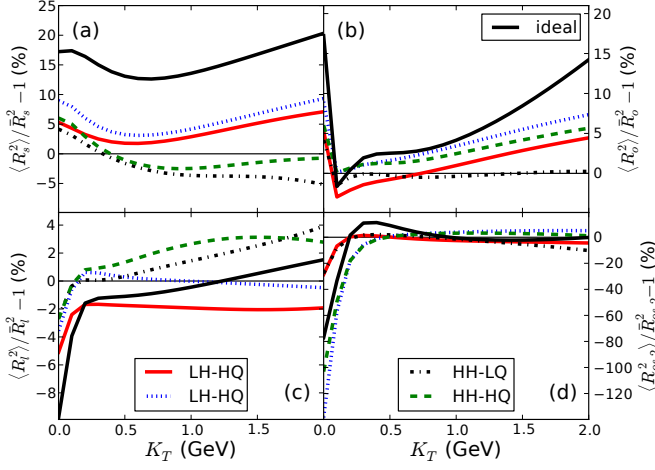


FIG. 6: The fractional change $(\langle R_{ij}^2 \rangle - \bar{R}_{ij}^2) / \bar{R}_{ij}^2$ of the squared HBT radii due to event-by-event fluctuations, as a function of pair momentum K_T . See text for discussion.

radii by a few percent above the corresponding radii obtained from single-shot hydrodynamic evolution of a smooth averaged initial condition. Exceptions to this rule are the sideward radius for the HH-LQ and HH-HQ parametrizations (i.e., for large shear viscosities at freeze-out) in the range $K_T > 0.5$ GeV, driven by effects from the δf correction at freeze-out, and the longitudinal radius at small pair momentum $K_T < 0.2$ GeV. The systematic effects of event-by-event fluctuations on the mean Φ_K -oscillation amplitude $\langle R_{os,2}^2 \rangle$ are less unambiguous, with fluctuations increasing or decreasing $\langle R_{os,2}^2 \rangle$ relative to $\bar{R}_{os,2}^2$ in different K_T -ranges depending on the specific temperature dependence selected for $(\eta/s)(T)$; the differences can become substantial at small K_T where the oscillation amplitude is small, with $\langle R_{os,2}^2 \rangle$ even changing sign relative to $\bar{R}_{os,2}^2$ in the LH-HQ and HH-HQ parametrizations. Generically the differences between the mean fluctuating HBT radii and their single-shot hydrodynamic analogs are largest for ideal fluid evolution and somewhat smaller for viscous evolution. This is consistent with the idea that viscosity attenuates fluctuation-driven effects.

For a better understanding of how different temperature dependences of $(\eta/s)(T)$ affect the magnitudes and K_T dependences of the radius parameters \bar{R}_{ij}^2 and $\langle R_{ij}^2 \rangle$ we can look directly at the emission functions. These are shown in Fig. 7a for a randomly selected single fluctuating event, and in Fig. 7b for the single-shot hydrodynamic event with smooth ensemble-averaged initial conditions. Having seen in Figs. 2-5 that at RHIC energies the HBT radii discriminate mostly between $(\eta/s)(T)$ parametrizations that differ in the value of η/s at the earliest times and highest temperatures, we focus in Fig. 7b on the HH-LQ and HH-HQ parametrizations (a comparison of LH-LQ with LH-HQ would lead to similar conclusions).

As is well known (see, e.g., Ref. [34]), the average radial flow velocity increases approximately linearly with r as one moves from the top of the freeze-out surface in Fig. 7b (at $r=0$) to its vertical part (where $r=r_{\max}$ takes its maximum value). For the cases studied in Fig. 7, this is shown in Fig. 8. This observation explains why, for increasing K_T , the region of maximal emissivity (colored red) moves from around $r=0$ for small momentum pairs to r_{\max} for large momentum pairs. Fig. 7a illustrates how this phenomenon manifests itself in an individual fluctuating event: While the regions of highest emissivity roughly follow the average tendencies seen in Fig. 7b, these tendencies are strongly modulated by fluctuations in the shape of the freeze-out surface and of the radial flow along this surface, giving rise to peaks and valleys of emissivity as one moves around the freeze-out surface at constant values of r or τ . Fig. 7a also illustrates that, in an individual event, the regions of maximal emissivity have a strong dependence on the azimuthal direction Φ_K of pair emission, and that therefore, for an individual fluctuating event, one should expect strong Φ_K -dependence of the HBT radius parameters.

Comparing the freeze-out surfaces and regions of maximal emissivity shown in Fig. 7b for the two ensemble-averaged sources that were evolved with shear viscosities $(\eta/s)(T)$ differing only in their behavior at high temperatures, we can make several observations:

- (1) The larger specific shear viscosity of the HH-HQ parametrization drives stronger radial flow which causes the fireball to expand to larger radii and complete its freeze-out at earlier times than for the HH-LQ parametrization. This agrees with similar observations made in Ref. [20].
- (2) For longitudinally boost-invariant expansion with longitudinal velocity component $v_z = z/t$, emissivity regions centered at later times see a smaller longitudinal flow gradient and thus a larger longitudinal region of homogeneity, reflected in a larger value for R_l^2 [12]. Fig. 7b shows that maximal emissivity for small and intermediate K_T pairs is shifted to later times for the HH-LQ parametrization than for HH-HQ, while for large $K_T = 2$ GeV the pairs are emitted at roughly the same times for both parametrization. This explains why in Figs. 2c (and also in Fig. 4c) the longitudinal HBT radii are larger for HH-LQ than for HH-HQ at small and intermediate K_T but nearly identical at large K_T .
- (3) For small K_T , the regions of highest emissivity are geometrically smaller in the outward and sideward⁴ directions for the HH-LQ case than for HH-HQ, but the opposite is true at intermediate and high pair momentum. This explains the behavior of the sideward radius R_s^2 for these two parametrizations shown in Figs. 2a.

⁴ To see the truth of this second statement the reader should in her mind visualize the emission surface rotated in ϕ direction and look at its horizontal width when frontally viewed.

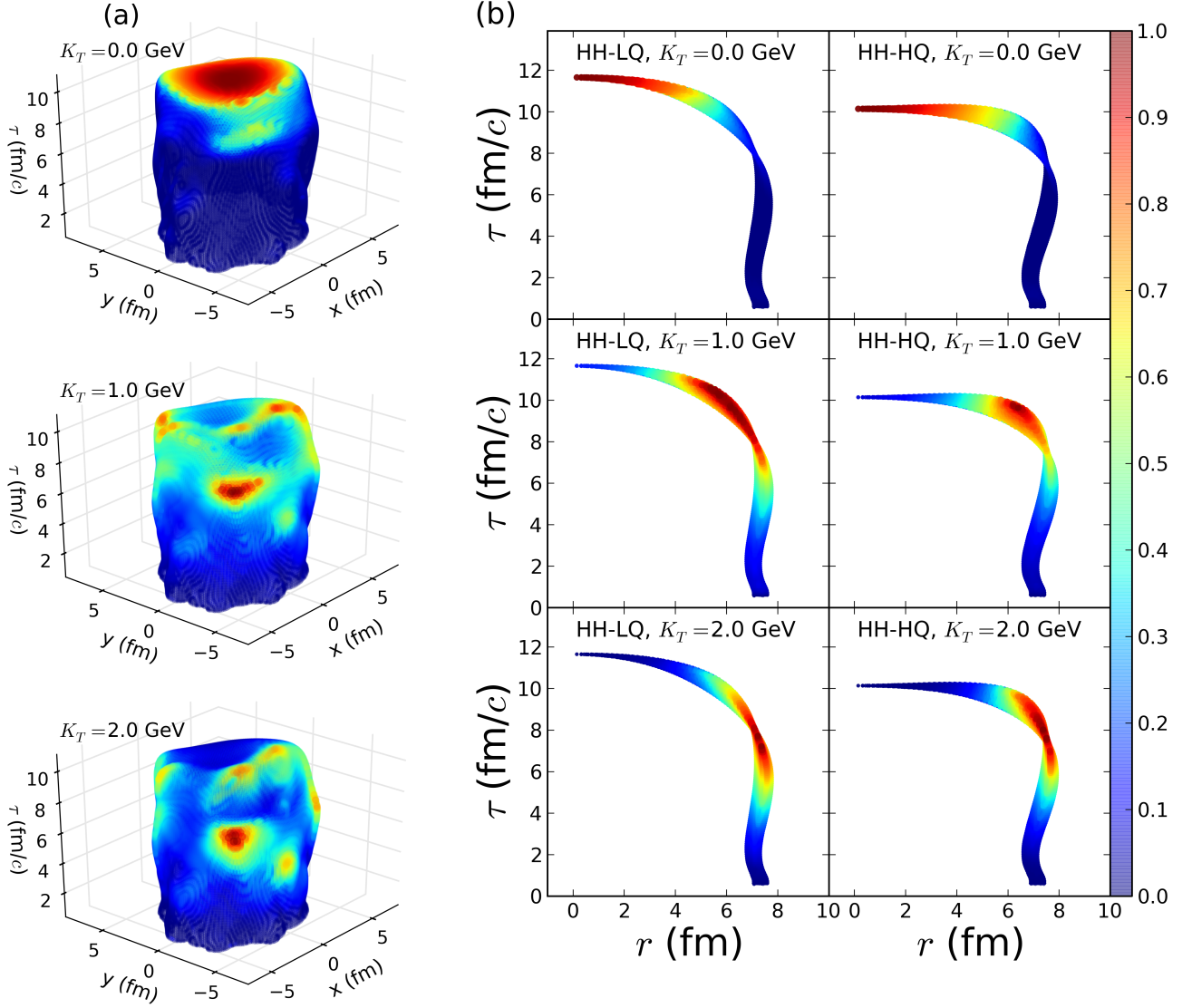


FIG. 7: (a) The emission function $S(x, K)$, for three values of K_T as indicated, $Y=0$ and integrated over Φ_K and η_s , for a single fluctuating event from the 0-10% centrality range, evolved with $(\eta/s)_{\text{HH-LQ}}$. Colors code the emission intensity, normalized to its maximum value on the freeze-out surface. (b) The emission function $S(x, K)$ for the smooth average single-shot hydrodynamic event corresponding to 0-10% centrality, for the same three values of K_T , $Y=0$ and integrated over Φ_K and η_s , using the same color code as in (a). The width of the bands arises from plotting the (τ, r) freeze-out contours for all spatial angles ϕ_s on top of each other. The left and right columns of panels show results for evolution with $(\eta/s)_{\text{HH-LQ}}$ and $(\eta/s)_{\text{HH-HQ}}$, respectively. See text for discussion.

The most important aspect of the freeze-out surfaces shown in Figs. 7b is the earlier freeze-out associated with larger shear viscosities at early times (high temperatures). It reduces the emission duration and increases the longitudinal flow gradient at freeze-out, which reduces the $\langle \tilde{x}_l^2 \rangle_S$ and $\langle \tilde{t}^2 \rangle_S$ contributions to R_l^2 and R_o^2 in Eqs. (10), (11) and is the root cause for the robustly smaller R_o^2 and R_l^2 values observed in Figs. 2b-c and 4b-c for the HH-HQ parametrization of $(\eta/s)(T)$ compared to the HH-LQ case. Its effect on the cross-terms variances

$\langle \tilde{x}_o \tilde{x}_s \rangle_S$, $\langle \tilde{x}_o \tilde{t} \rangle_S$ and $\langle \tilde{x}_s \tilde{t} \rangle_S$ (and thus the behavior of the cross-term radius R_{os}^2) is less intuitively obvious.

Last but not least, it is well established that the rate at which R_s^2 decreases with increasing pair momentum K_T is a measure of the radial velocity gradient along the freeze-out surface [12]. Comparison of Figs. 8b,e,h (middle column) to Figs. 8c,f,i (right column) shows that evolution with $(\eta/s)_{\text{HH-HQ}}$ leads to a larger radial flow gradient along the freeze-out surface than evolution with $(\eta/s)_{\text{HH-LQ}}$ (which has smaller shear viscosity at early

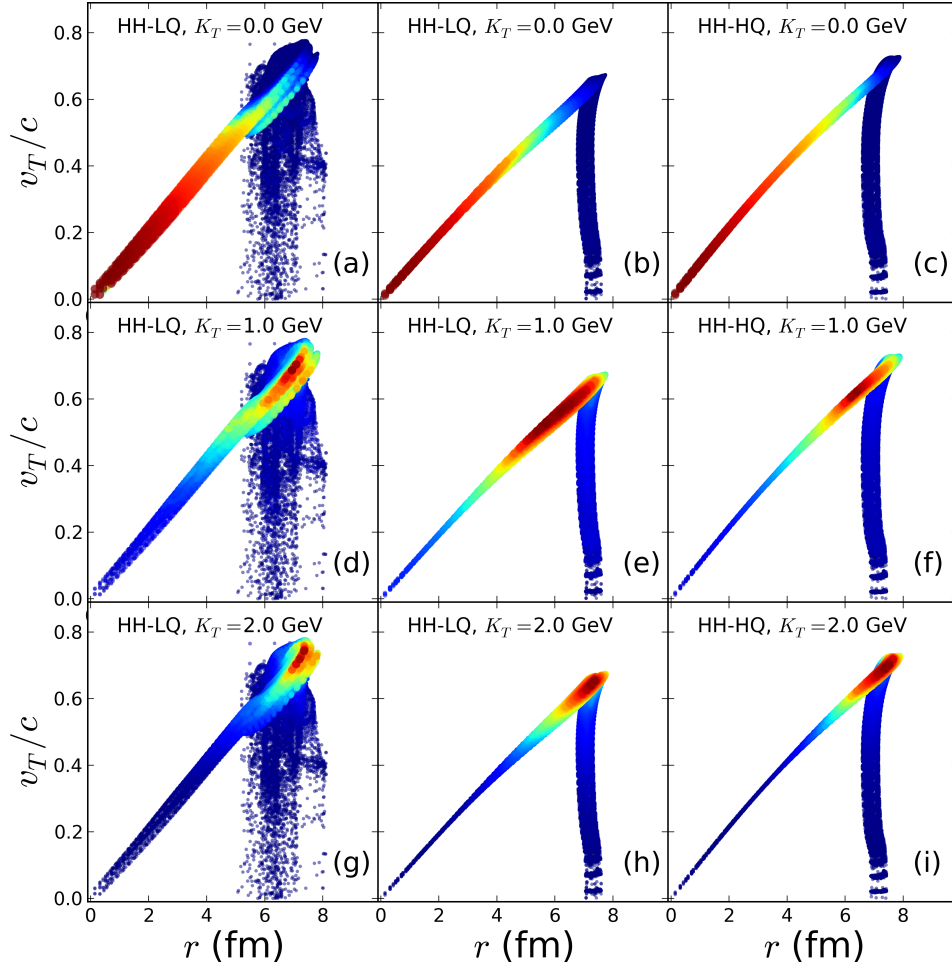


FIG. 8: For each cell on the freeze-out surface the radial velocity is plotted against its radial position, color coded as in Fig. 7 for its emission intensity normalized by its maximal value on the surface. Panels a,d,g in the left column are for the single fluctuating event, evolved with $(\eta/s)_{\text{HH-LQ}}$, shown in Fig. 7a, for the same three K_T values as indicated. Panels b,e,h in the middle column and panels c,f,i in the right column are for the ensemble-averaged event shown in Fig. 7b, evolved with single-shot hydrodynamics using $(\eta/s)_{\text{HH-LQ}}$ (middle column) and $(\eta/s)_{\text{HH-HQ}}$ (right column), respectively. See text for discussion.

times). This correlates with the steeper K_T dependence for R_s^2 in Figs. 2a and 4a for the HH-HQ parametrization (green dashed curves) than for the HH-LQ one (black dash-dotted curves).

B. Variances of HBT radii and their K_T dependence

Finally, we consider the variances of the event-by-event distributions of the HBT radii. We present them in the form of *relative* widths, normalized to the directly ensemble averaged squared radii, in Figures 9 (full freeze-out distribution function) and 10 (without the viscous δf correction on the freeze-out surface). For the Φ_K -averaged radius parameters the relative widths are seen to be of order 10 – 15%, with little dependence on either K_T or the specific shear viscosity used in the hydrody-

namical evolution. The event-by-event distribution of the out-side oscillation amplitude $R_{os,2}^2$ shows a somewhat smaller relative width, especially at small K_T where the mean amplitude is small. At larger K_T , shear viscosity appears to reduce the relative width of the event-by-event distribution of this oscillation amplitude compared to ideal fluid evolution.

Focusing on the Φ_K -averaged radii (panels (a-c) in Figs. 9 and 10) we observe that, just as was the case for their ensemble averages, all sensitivity of their variances to the temperature dependence of η/s in the hadronic phase appears to come from the viscous δf correction at freeze-out and thus not to be of dynamical origin. The sensitivity of the HBT variances to dynamical evolution effects caused by varying the temperature dependence of η/s at temperatures above freeze-out can be seen in Fig. 10 where the δf contribution at freeze-out is removed. The results for viscous evolution split into two

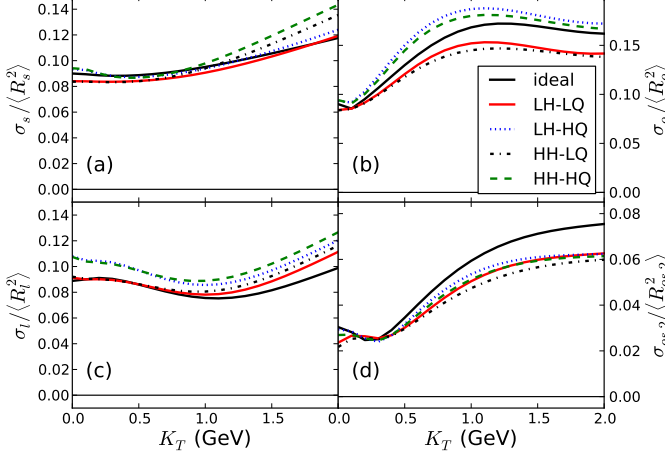


FIG. 9: The normalized widths of the event-by-event distributions of HBT radii as functions of pair momentum K_T , for ideal fluid evolution and viscous dynamics with the four parametrizations shown in Fig. 1.

bands, one for high, the other for low shear viscosity at early times. The relative widths for ideal fluid dynamics fall in between these two bands. The two bands are characterized by the behavior of η/s at *high* temperature, not at low T : Higher shear viscosity at early times (i.e. at high temperatures) leads to HBT variances that are 10-20% larger than those for evolution with lower shear viscosity at early times. The behavior of the shear viscosity at late times in the hadronic phase has no visible dynamical effect on the normalized widths of the HBT radii.

IV. CONCLUSIONS

We have presented a first analysis of the sensitivity of the HBT radii to the temperature dependence of the specific shear viscosity in relativistic heavy ion collisions at top RHIC energies, taking into account that the HBT radii fluctuate from event to event and that a consistent comparison of experimental data with theoretical predictions should thus be based on event-by-event evolution of fluctuating initial conditions on the theory side. We explored the effect of event-by-event fluctuations on the mean HBT radii (and their deviation from the values obtained from single-shot hydrodynamics where the initial-state fluctuations are ignored by averaging over them before hydrodynamic evolution) and their relative widths. We found that fluctuations tend to increase the mean value of the fluctuating HBT radii by a few percent above the value obtained by the traditional process of averaging over the fluctuations already in the initial state, and found that the event-by-event distributions of the HBT radii are characterized by relative widths of order 10%.

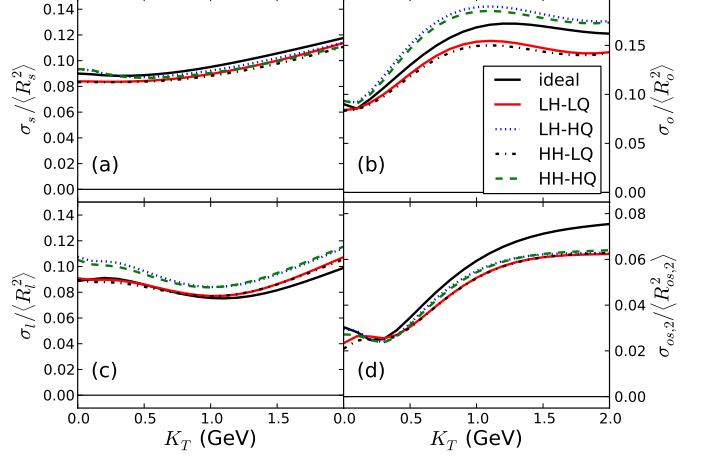


FIG. 10: Same as Fig. 9, but without the viscous correction δf to the freeze-out distribution function. One sees that for the normalized width of the distribution of sideward radii R_s^2 , deleting δf removes all sensitivity to the temperature dependence of η/s in the hadronic phase, while all other normalized widths are only weakly affected by δf .

Comparing the HBT radii from hydrodynamic evolutions with five different assumptions for the specific shear viscosity and its temperature dependence we showed that both the mean squared HBT radii and their relative widths are affected by a possible increase of the specific shear viscosity by a factor 10 between T_{tr} and $3T_{tr}$ at the level of 10-20%, with larger shear viscosities leading to smaller mean HBT radii and larger relative widths of their event-by-event distributions. There is little to no effect on either from variations in the behavior of $(\eta/s)(T)$ in the hadronic phase below T_{tr} , except for the sideward and out-side radius parameters R_s^2 and $R_{os,2}^2$ and the sideward variance σ_s^2 which all show significant sensitivity to the viscous δf correction at freeze-out. The latter, in turn, depends on the value of η/s at the freeze-out temperature but not on its prior dynamical evolution in the hadronic phase. Since the δf correction is not theoretically well constrained at the present moment, this sensitivity of R_s^2 and $R_{os,2}^2$ to η/s at freeze-out should be viewed with some caution.

The levels of sensitivity of the HBT radii and their variances to the temperature dependence of η/s observed here are comparable to those observed in Ref. [1] for the elliptic and quadrangular flows. This indicates that precise 3-dimensional HBT measurements, in particular new measurements of their variances [9], can play a valuable supporting role in constraining the temperature dependence of the QGP shear viscosity.

Acknowledgments

The authors would like to thank Chun Shen for a careful reading of the manuscript which exposed an error in its original version. This work was supported by the

U.S. Department of Energy, Office of Science, Office of Nuclear Physics under Awards No. DE-SC0004286 and (within the framework of the JET Collaboration) DE-SC0004104.

-
- [1] E. Molnar, H. Holopainen, P. Huovinen and H. Niemi, Phys. Rev. C **90**, 044904 (2014).
 - [2] I. G. Bearden *et al.*, Phys. Rev. C **58**, 1656 (1998).
 - [3] D. Adamova *et al.* [CERES Collaboration], Nucl. Phys. A **714**, 124 (2003).
 - [4] B. B. Abelev *et al.* [ALICE Collaboration], Phys. Rev. C **89**, 024911 (2014).
 - [5] L. Adamczyk *et al.* [STAR Collaboration], arXiv:1403.4972 [nucl-ex].
 - [6] A. Adare *et al.* [PHENIX Collaboration], arXiv:1410.2559 [nucl-ex].
 - [7] J. Adam *et al.* [ALICE Collaboration], Phys. Rev. C **91**, 034906 (2015).
 - [8] C. J. Plumberg, C. Shen and U. Heinz, Phys. Rev. C **88**, 044914 (2013) [Erratum-ibid. C **88**, 069901 (2013)].
 - [9] C. Plumberg and U. Heinz, manuscript in preparation.
 - [10] U. A. Wiedemann and U. Heinz, Phys. Rept. **319**, 145 (1999).
 - [11] P. F. Kolb and U. Heinz, in *Quark-Gluon Plasma 3*, R. C. Hwa *et al.* (Eds.) (World Scientific, Singapore, 2004), pp. 634-714 [arXiv:nucl-th/0305084].
 - [12] U. Heinz and B. V. Jacak, Ann. Rev. Nucl. Part. Sci. **49**, 529 (1999).
 - [13] M. A. Lisa and S. Pratt, in *Relativistic Heavy Ion Physics*, R. Stock (Ed.), Landolt-Börnstein I **23**, 653-685 (2010) (Springer, Heidelberg) [arXiv:0811.1352 [nucl-ex]].
 - [14] A. Kisiel, W. Florkowski, W. Broniowski and J. Pluta, Phys. Rev. C **73**, 064902 (2006).
 - [15] P. Romatschke, Eur. Phys. J. C **52**, 203 (2007).
 - [16] P. Bozek and I. Wykiel, Phys. Rev. C **79**, 044916 (2009).
 - [17] E. Frodermann, U. Heinz and M. A. Lisa, Phys. Rev. C **73**, 044908 (2006).
 - [18] C. Shen, Z. Qiu, H. Song, J. Bernhard, S. Bass and U. Heinz, arXiv:1409.8164 [nucl-th].
 - [19] B. Alver, M. Baker, C. Loizides and P. Steinberg, arXiv:0805.4411 [nucl-ex].
 - [20] H. Song and U. Heinz, Phys. Rev. C **77**, 064901 (2008).
 - [21] C. Shen, U. Heinz, P. Huovinen and H. Song, Phys. Rev. C **82**, 054904 (2010).
 - [22] S. Pratt, Phys. Rev. Lett. **102**, 232301 (2009); and Nucl. Phys. A **830**, 51C (2009).
 - [23] F. Cooper and G. Frye, Phys. Rev. D **10**, 186 (1974).
 - [24] B. R. Schlei, U. Ornik, M. Plumer and R. M. Weiner, Phys. Lett. B **293**, 275 (1992).
 - [25] S. Chapman and U. Heinz, Phys. Lett. B **340**, 250 (1994).
 - [26] D. Teaney, Phys. Rev. C **68**, 034913 (2003).
 - [27] K. Dusling, G. D. Moore and D. Teaney, Phys. Rev. C **81**, 034907 (2010).
 - [28] C. Gombeaud, T. Lappi and J. Y. Ollitrault, Phys. Rev. C **79**, 054914 (2009).
 - [29] J. E. Bernhard, P. W. Marcy, C. E. Coleman-Smith, S. Huzurbazar, R. L. Wolpert and S. A. Bass, arXiv:1502.00339 [nucl-th].
 - [30] Z. Qiu and U. Heinz, Phys. Rev. C **84**, 024911 (2011).
 - [31] U. Heinz and R. Snellings, Ann. Rev. Nucl. Part. Sci. **63**, 123 (2013).
 - [32] U. Heinz, A. Hummel, M. A. Lisa and U. A. Wiedemann, Phys. Rev. C **66**, 044903 (2002).
 - [33] A. Tamhane and D. Dunlop, *Statistics and Data Analysis: from Elementary to Intermediate* (Pearson/Prentice-Hall, 2000).
 - [34] D. Teaney, J. Lauret and E. V. Shuryak, arXiv:nucl-th/0110037.